







Superconducting LaP_2H_2 with graphenelike phosphorus layers

Xing Li ^{1,*}, Xiaohua Zhang ^{1,2,*}, Aitor Bergara ^{3,4,5}, Guoying Gao ⁶, Yong Liu ¹, and Guochun Yang ^{1,2,†}

¹State Key Laboratory of Metastable Materials Science & Technology and Key Laboratory for Microstructural Material Physics of Hebei Province, School of Science, Yanshan University, Qinhuangdao 066004, China

²Centre for Advanced Optoelectronic Functional Materials Research and Key Laboratory for UV Light-Emitting Materials and Technology of Northeast Normal University, Changchun 130024, China

³Departamento de Física, Universidad del País Vasco-Euskal Herriko Unibertsitatea, UPV/EHU, 48080 Bilbao, Spain

⁴Donostia International Physics Center (DIPC), 20018 Donostia, Spain

⁵Centro de Física de Materiales CFM, Centro Mixto CSIC-UPV/EHU, 20018 Donostia, Spain

⁶Center for High Pressure Science (CHiPS), State Key Laboratory of Metastable Materials Science and Technology, Yanshan University, Qinhuangdao 066004, China



(Received 14 October 2021; revised 9 December 2021; accepted 14 December 2021; published 6 January 2022)

Novel structural building blocks in compounds could induce interesting physical and chemical properties. Although phosphorus tends to form very different motifs, the existence of lone pair electrons has always prevented the formation of graphenelike structures. Here, the application of first-principles swarm structural calculations has allowed us to predict the stability of pressure-induced hexagonal LaP_2H_2 containing graphenelike phosphorus, which derives from the trigonal bipyramid configuration of P atoms regulated by symmetric hydrogen bonds. LaP_2 in LaP_2H_2 has the same configuration as MgB_2 , and P and H atoms form a three-dimensional framework as H_3S . Interestingly, LaP_2H_2 shows a superconductivity dominated by the graphenelike phosphorus layer and its coupling with La atoms. On the other hand, LaP_2H_2 is not only superconducting at a lower pressure than the H-rich LaPH_6 , but it also shows a superconducting transition temperature three times higher. Our work provides an example which extends the landscape of conventional superconductors at lower pressures.

DOI: [10.1103/PhysRevB.105.024504](https://doi.org/10.1103/PhysRevB.105.024504)

The search for conventional superconductors has recently achieved a breakthrough, approaching the goal of room-temperature superconductivity [1–4]. Basic atomic building blocks in superconductors, such as hydrogen cages in LaH_{10} [5] and pentagraphenelike hydrogen in HfH_{10} [3], are decisive for this high-temperature superconductivity, which can be described by the Bardeen-Cooper-Schrieffer (BCS) theory [6], offering a clear guide for designing new superconducting materials [5,7,8]. Notably, first-principles calculations, combined with computational structural searches, play a key role in understanding the origin of superconductivity and in accelerating the discovery of superconductors [9–14].

MgB_2 became the milestone of BCS superconductors with an enhanced T_c of 39 K [15], where B atoms adopt a graphenelike configuration with a σ bonding in the boron plane, due to the sp^2 hybridization, and a delocalized π bonding out of the boron plane, via the p_z orbital hybridization [16]. Remarkably, the graphenelike boron layer induces a strong electron-phonon coupling (EPC), which is responsible for its superconducting transition [17,18].

Later, H_3S became the prototype of pressure-induced covalent hydride superconductors, displaying a remarkably high T_c of 203 K at 155 GPa [1], reawakening the dream of room-temperature superconductivity [19,20]. H_3S shows an extraordinary structure, with H atoms symmetrically bonded

to two S atoms in the body centered cubic sublattice, forming a three-dimensional (3D) framework [7]. The high-frequency H vibration mode induced by the covalent framework enhances the EPC responsible for superconductivity [21].

Additionally, the LaH_{10} clathrate represented another kind of high- T_c superconducting hydride, consisting of sodalitelike hydrogen cages [5] and a face centered cubic La sublattice stabilized by covalent and ionic interactions [22]. The H-derived high-frequency phonon mode strongly couples with La f and H s electronic states near the Fermi level (E_F) [23], yielding an exciting high T_c of 260 K at 188 GPa [2].

On the other hand, it is well known that phosphorus (P) can form abundant allotropes [24] (e.g., white, black, and blue phosphorus) and diverse motifs [25] in its compounds (e.g., chains, rings, cages, and tubular frameworks). The appearance of nonplanar P configurations is one of their common characteristics, which is due to the repulsion between lone electron pairs and bonding electrons. In P-rich metal phosphides, P building units can be modulated by metallic elements, which is attributed to their different radii and electropositivities, and are closely related to superconductivity [26–28]. For instance, $Pnma$ Nb_2P_5 with zigzag P chains shows a T_c of 2.6 K at 0 GPa [26]; the T_c of $I4/mmm$ KP_2 , consisting of puckered layers of P_4 rings, goes up to 22 K at 5 GPa [27], and $Cmmm$ MgP_2 , stabilized by a three-dimensional P covalent network, has a T_c of 10.2 K at 150 GPa [28]. Therefore, the discovery of novel P motifs might provide an opportunity to find new superconductors with an enhanced T_c .

*These authors contributed equally to this work

†Corresponding author: yanggc468@nenu.edu.cn

In addition, P is adjacent to S in the periodic table and both have similar electronegativities, thus, after the discovery of superconducting H_3S , P-H compounds were also considered as potential high- T_c superconductors. First, Drozdov *et al.* [29] observed experimentally a T_c of 103 K in compressed PH_3 at 207 GPa. However, its crystal structure and superconducting origin have not been unequivocally clarified. Several theoretical works found that all the considered P-H stoichiometries are thermodynamically metastable with respect to the decomposition into elemental P and solid H_2 [30–33]. Interestingly, some candidate phases have calculated T_c values comparable to the measured ones (76 K for $C2/m$ PH_2 at 200 GPa [30], 78 K for $I4/mmm$ PH_2 at 220 GPa [31], and 83 K for $C2/m$ PH_3 at 200 GPa [32]). Unlike pressure-induced H_3S , metastability of PH_3 could be attributed to the fact that P has one valence electron ($3s^23p^3$) less than S ($3s^23p^4$).

Based on a physicochemical intuition, the insertion of metal atoms combined with variable pressures has become a strategy to improve the stability of the P-H system [34–36]. For example, several Li-P-H ternary compositions were predicted to be stable at high pressures [34,35]. Even more interestingly, two high- T_c superconductors were proposed, $Pm-3$ LiPH_6 with a T_c of 167 K at 200 GPa and $R-3$ $\text{LiP}_2\text{H}_{14}$ with 169 K at 230 GPa, where superconductivity is associated with a strong EPC of H-derived high-frequency vibrations, similar to H_3S . Later, $R-3m$ TiPH_4 was predicted to have a T_c of 62 K at 250 GPa, closely related to the low-frequency vibrations of Ti and P atoms [36]. Until now, these studies focused on H-rich compositions. However, considering the fascinating characteristics of P, as mentioned above, there are expectations of stabilizing ternary compounds with novel P motifs by modulating the ratio of P and H, which may offer an opportunity to design new superconducting materials and understand the interplay of P motifs and H atoms on the superconducting mechanism.

La atom has a strong ability to donate electrons, stabilizing H cages and ternary hydrides, such as LaN_2H_3 [37] and LaBH_8 [37–39]. On the other hand, there appears puckered P layers composed of P_{12} rings [40] in LaP_5 at ambient pressure. We cannot help but imagine whether introducing La atoms combined with pressure could result in the stable La-P-H compounds with novel P motifs and charming superconductivity. As expected, LaP_2H_2 , consisting of a hitherto unknown graphenelike P configuration, becomes stable above 100 GPa. More interestingly, the graphenelike P layer and its coupling with La atoms are mainly responsible for the superconducting transition, analogous to the B layer in MgB_2 . The T_c value of 36.3 K at 125 GPa in LaP_2H_2 is much higher than the T_c of 10.4 K at 200 GPa in H-rich LaPH_6 .

Our structural search was performed by employing an intelligence-based particle-swarm optimization algorithm [41], as described in the Supplemental Material [49]. Reliable determination of the phase stability of ternary compounds requires knowledge on the stable structures of constituent elemental solids and binary compounds. The high-pressure phase diagrams of La-H [5,8,42,43] and P-H [30–33] systems, as well as their elemental solids (La [44,45], P [46], and H_2 [47]) are already known. However, stable La-P compositions at high pressures have so far rarely been explored [48]. Therefore, we first explored the stability of La-P compounds (Fig. S1 in the

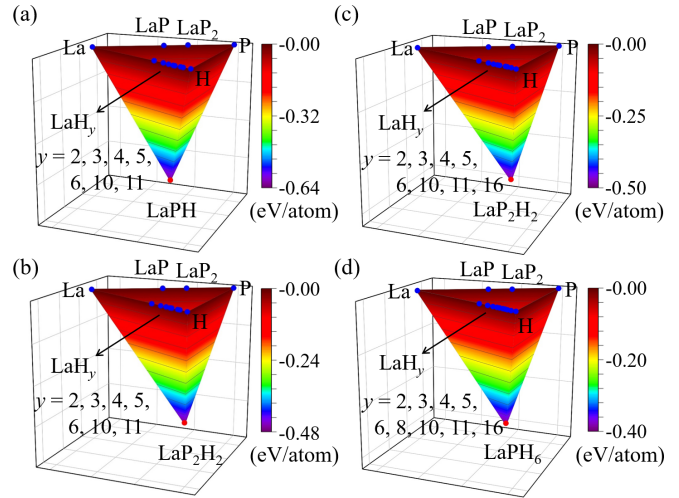


FIG. 1. Calculated stabilities of LaP_xH_y derived from their formation enthalpies (ΔH) relative to elemental solids and binary compounds at (a) and (b) 100 GPa, (c) 125 GPa, and (d) 150 GPa. To highlight the stability of predicted ternary compounds, the elements and stable binary phases are indicated by blue circles, and their ΔH values are projected onto the plane of 0 eV.

Supplemental Material [49]). The detailed structural characteristics and properties of stable binary La-P compounds will be reported elsewhere.

Taking into account both the high- T_c H-rich compounds and the role of P motifs in the superconducting transition, we focused our structural search on P-rich and H-richer compounds. Energetic stabilities of a plethora of LaP_xH_y ($x = 1-3$, $y = 1-8$) compounds are evaluated by their formation enthalpies relative to the dissociation into constituent elements and binary compounds at 100, 125, and 150 GPa. As shown in the convex hull diagrams (Fig. 1), three chemical compositions, LaPH , LaP_2H_2 , and LaPH_6 , become thermodynamically stable.

LaP_2H_2 crystallizes into a hexagonal structure (space group $P6/mmm$) at 100 GPa. LaPH and LaPH_6 stabilize into an orthorhombic structure with space groups $Pnma$ at 100 GPa and $Pmnm$ at 150 GPa, respectively. The three stable phases are dynamically stable as well, due to the absence of imaginary frequencies in their phonon dispersion curves (Fig. S2 [49]). Compared to Li-P-H and Ti-P-H systems [34–36], besides H-rich composition, P-rich LaP_2H_2 also emerges.

In addition to the difference in composition between La-P-H and Li/Ti-P-H [34–36], the three stable La-P-H compounds exhibit unique structural and bonding characteristics. Specifically, in LaP_2H_2 [Fig. 2(a)] P atoms form a desirable graphenelike configuration through an equivalent threefold coordination in the ab plane [Fig. 2(b)]. The H atoms are symmetrically distributed between the two adjacent P planes, and each H atom bonds with two P atoms along the c axis, forming a 3D P-H covalent framework. Thus, P atoms show a trigonal bipyramid configuration, as appeared in PCl_5 [61]. However, the sp^2 hybridization in the P plane and the two left electrons sitting in the p_z orbitals that bond with two H atoms are in stark contrast with the sp^3d hybridization in PCl_5 . This is supported by the absence of a P d orbital contribution and a

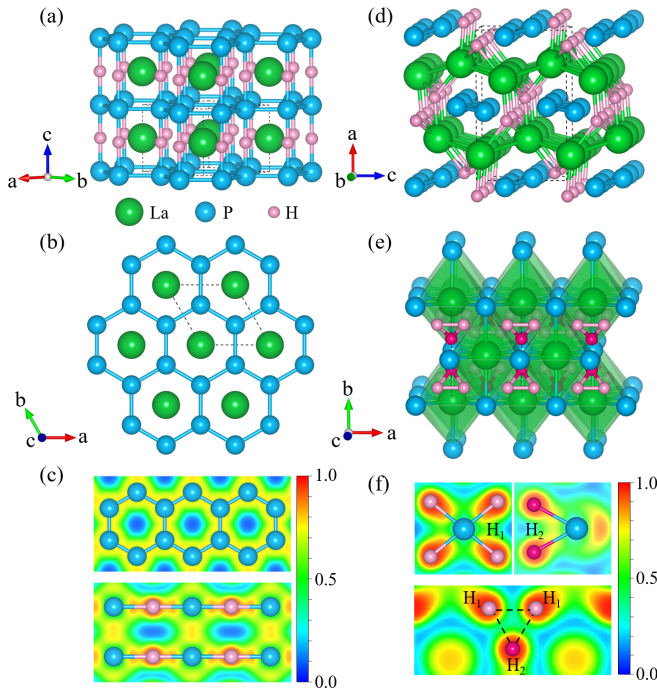


FIG. 2. The crystal structure of $P6/mmm$ LaP_2H_2 at 125 GPa in (a) side and (b) top view, (d) $Pnma$ LaPH at 100 GPa, and (e) $Pmnm$ LaPH_6 at 200 GPa. The ELF maps of (c) LaP_2H_2 on the (001) and (110) planes, and (f) LaPH_6 .

strong overlap between P p_z and H s orbitals in the projected density of states (Fig. S3 [49]). The P-P and P-H bond lengths are 2.11 and 1.66 Å at 125 GPa, respectively, which are within the range of a covalent bonding [30–32,62], as is confirmed by the electron localization functional (ELF) [Fig. 2(c)]. In addition to the same arrangement of La and P atoms with respect to Mg and B, respectively, in MgB_2 , each La atom coordinates with six H atoms.

On the other hand, the atomic arrangement of the symmetric P-H-P differs remarkably from those of binary P-H [30–32] and ternary Li/Ti-P-H compounds [34–36]. Symmetric hydrogen bonding has played an important role in raising the H vibration frequency and strengthening the EPC, as in H_3S [7], and BH [63] compounds. Such unique structure of LaP_2H_2 is stabilized by a charge transfer from La to P and H atoms, which facilitates the formation of symmetric hydrogen bonds. The Bader charge analysis [64] shows that each La atom loses $1e^-$, and that both P and H atoms accept $0.3e^-$ and $0.2e^-$, respectively. Considering that a P atom just needs five valence electrons to form fivefold covalent bonds, the electrons donated by La atoms might occupy P-P antibonding orbitals under pressure, which is confirmed by the enhancement of localized electrons between P-P bonds after removing La atoms [Fig. S4(a)].

$Pnma$ LaPH [Fig. 2(d)] contains puckered La layers in the bc plane, in which H atoms are located at the interlayer region, forming HLa_4 tetrahedra with La atoms in adjacent La layers. Interestingly, the HLa_4 tetrahedra are arranged alternately sharing edges along the b -axis direction, making spiral hexagonal channels. In the channels, P atoms show a zigzag-chain configuration with a P-P bond length of 2.12 Å. Bader charge

analysis and the ELF map [Fig. S4(b)] indicate that P atoms accept electrons from La atoms and are covalently bonded via sp^3 hybridization. The shortest distance between P and H atoms is 2.12 Å, which is much longer than their covalent bond range [30–32], and means negligible P-H interaction.

In $Pmnm$ LaPH_6 [Fig. 2(e)], the edge-sharing distorted LaP_6 octahedra make a tetrahedron cavity to accommodate triangular H units. Each H triangle consists of two inequivalent H's, labeled as H_1 and H_2 atoms, with interatomic distances of 1.36 Å for H_1 - H_1 , and 1.35 Å for H_1 - H_2 . Such a unique H triangle is stabilized by strong P- H_1 and weak P- H_2 polar covalent bonds, with distances of 1.46 and 1.61 Å, respectively, as well as by a weak covalent interaction between H atoms [65,66], as identified by the ELF in Fig. 2(f). Apparently, these structural characteristics in LaPH_6 are distinct from the H-rich phases in Li/Ti-P-H systems, which usually contain PH_y polyhedra [34–36].

Calculations of electronic properties clearly indicate that the three stable phases are metallic. Among them, LaP_2H_2 has the highest electronic density of states (DOS) at the E_F at 125 GPa (Fig. S5). The projected electronic energy band of LaP_2H_2 [Fig. 3(d)] shows that the electronic states associated to La and P atoms are responsible for the metallicity, while H states are mainly located below the E_F hybridized with P states, which stabilizes the P-H framework. A clear orbital overlap of P s , p_x , and p_y states appears near the high symmetry point A (Fig. S5a), supporting the sp^2 hybridization. Additionally, there are steep bands along the Γ -A and A-H directions and a flat band around the Γ point near the E_F , corresponding to a large DOS.

To further analyze the electronic properties of LaP_2H_2 , we also study the Fermi surfaces [Figs. 3(a)–3(c)] associated with the three bands that contribute significantly at the E_F . One of the Fermi surfaces shows a horn shape [Fig. 3(a)] and the other two have cylindrical features [Figs. 3(b) and 3(c)], which are quite similar to the topology of the Fermi surfaces in MgB_2 [16], confirming the similarities between LaP_2H_2 and MgB_2 (Figs. S7a–S7c). In detail, the horn-shaped Fermi surface in LaP_2H_2 is mainly derived from P p_z orbitals, which is similar to the B p_z orbital in MgB_2 . One of the cylindrical Fermi surfaces in LaP_2H_2 arises largely from a hybridized state of La d (d_{xz} and d_{z^2})/ f (f_{xyz} , f_{xz^2} , and $f_{x(x^2-3y^2)}$) and P s/p orbitals [Figs. 3(b), S8, and S9], while the other is dominated by a mixed state of La d (d_{xy} and $d_{x^2-y^2}$)/ f (f_{z^3} and $f_{z(x^2-y^2)}$) and P s/p (p_x and p_y) orbitals [Figs. 3(c), S8, and S9], which is different from the contribution of the B s/p (p_x and p_y) orbitals in MgB_2 [16].

The unique crystal structure and electronic properties encourage us to explore the superconductivity of LaP_2H_2 . The calculated EPC parameter (λ) of LaP_2H_2 is 0.90 at 125 GPa [Fig. 3(e)], where the vibrations of pure P and H atoms contribute 31% and 16% to the total λ in the range 9–18 and 29–48 THz, respectively; and the coupling between P and La atoms (below 9 THz) and P and H atoms (18–29 THz) contribute 32% and 21%, respectively. The origin of superconductivity in LaP_2H_2 is different from MgB_2 or H_3S . The role of the graphenelike P is similar to the B layer in MgB_2 , whereas the La-P coupling becomes much stronger than Mg-B and even comparable to graphenelike P. On the other hand, the contribution of high-frequency H vibrations to λ (16%)

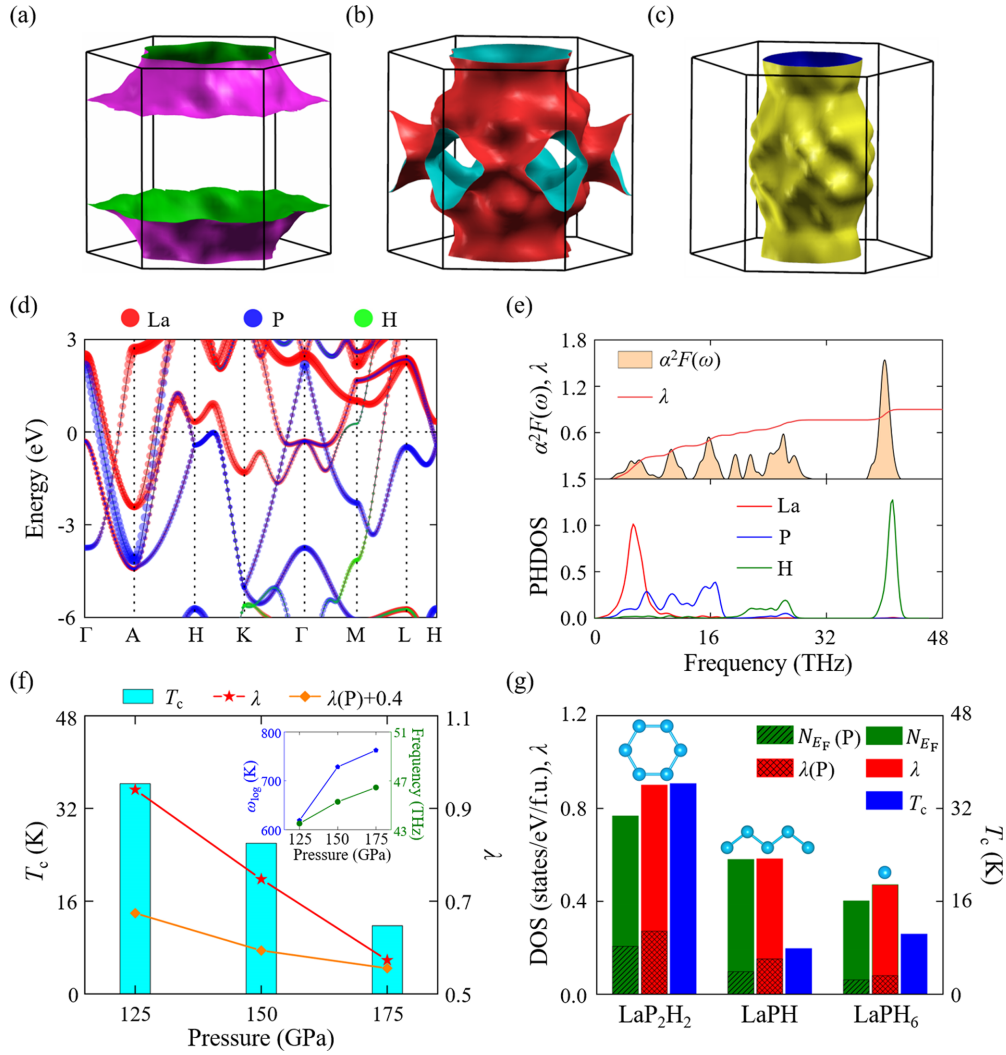


FIG. 3. (a)–(c) The three considered Fermi surfaces (the rest are in Fig. S6), (d) the projected electronic band structure, (e) the projected phonon density of states and Eliashberg spectral function of $P6/mmm$ LaP₂H₂ at 125 GPa. (f) Pressure dependence of T_c , the total EPC parameter λ and the contribution of P atoms to the total λ , namely $\lambda(P)$, for LaP₂H₂. The inset shows the evolution of the logarithmic average phonon frequency ω_{log} and the highest phonon frequency of H with pressure. (g) Calculated λ , $\lambda(P)$, and the DOS at the E_F projected on P atomic orbitals, $N_{E_F}(P)$.

is much smaller than 82.6% in H₃S [7]. Considering that the Allen-Dynes modified McMillan equation gives a better description of superconductors with $\lambda < 1.5$ [50], we applied it to calculate the T_c of LaP₂H₂. The resulting T_c is 36.3 K at 125 GPa with a typical Coulomb pseudopotential parameter of $\mu^* = 0.1$, which is much higher than that of LaH₄ (5 K at 300 GPa) [5], YS₄H₄ (20 K at 200 GPa) [67], LaSH₆ (35 K at 300 GPa) [68], MgH₂ (23 K at 180 GPa) [69], and BH (21 K at 175 GPa) [63], with a higher H content than LaP₂H₂. This indicates that the presence of novel building units in compounds might be also an effective routine to boost the T_c at a relatively lower pressure.

Furthermore, we also analyzed the pressure-dependent superconductivity of LaP₂H₂ [Fig. 3(f)]. T_c decreases with pressure, showing the same trend as λ . In contrast, ω_{log} monotonously increases, which can be attributed to the fact that the P-H bond is easier to shorten than the P-P bond (Fig. S10), resulting in a higher frequency of H vibration.

Therefore, λ plays a decisive role in the T_c of LaP₂H₂. On the other hand, the P-P coupling always accounts for a large proportion of the total λ , and it is positively correlated with the total λ under different pressures [Fig. 3(f)]. Consequently, we can conclude that the contribution of the rigid P layer to superconductivity does not show a strong dependence with pressure.

For LaPH, with the lowest H content, its metallicity is dominated by La atoms in the puckered layers (Fig. S5d). For LaPH₆, with the highest content of H, the contribution of H atoms to the DOS at the E_F is the highest, but there is a clear difference between the contributions of H₁ and H₂ atoms (Fig. S5e). H₁ atoms show a strong contribution near the high symmetry point T, while H₂ atoms mainly contribute along the path U-R. On the other hand, phonon frequencies associated to H₁ atoms are higher than those of H₂ atoms (Fig. S11f), mainly due to the stronger polar covalent bond between H₁ and P atoms. The resulting λ of LaPH is 0.59

at 100 GPa, where the low-frequency vibrations of La atoms (below 8 THz) contribute 51% of the total λ . The λ of LaPH₆ is 0.47 at 200 GPa, mainly coming from the high-frequency vibrations of H atoms (above 20 THz, 63% of λ), especially of the H₁ atoms. The corresponding T_c values of LaPH and LaPH₆ are 8.0 and 10.4 K (Figs. S11d and S11e), respectively.

Comparing different high- T_c hydrides, H atoms generally show several typical structural characteristics, such as the H cages [5,8,9], 2D planes [3,65], or 3D covalent network with nonmetals [7,70]. All the H atoms in the La-P-H system are in the atomic form, but P atoms form various motifs and make a different contribution to T_c [Fig. 3(g)]. From LaP₂H₂, with graphenelike P, to LaPH, with zigzag P chains, passing by LaPH₆, with isolated P atoms, basically, the corresponding T_c decreases, which can be connected to the reduction of λ and the DOS at the E_F . Additionally, the graphenelike P configuration in LaP₂H₂ makes the EPC stronger than those in LaPH and LaPH₆ due to the enhancement of the coupling between La and P (Fig. S11). On the whole, the discovery of LaP₂H₂ with a graphenelike P and the highest T_c in La-P-H system promotes the correlation between new building blocks and novel superconductors.

In summary, our extensive first-principles structural searches for the La-P-H system under high pressure have identified three stable stoichiometries: *P6/mmm* LaP₂H₂, *Pnma* LaPH, and *Pmnn* LaPH₆, where P atoms appear forming

different building blocks. In LaP₂H₂, P atoms form graphenelike layers, in LaPH zigzag chains, and in LaPH₆ isolated P atoms are present. LaP₂H₂ is predicted to be a superconductor with an estimated T_c of 36.3 K at 125 GPa, which is much higher than the T_c predicted for LaPH₆, 10.4 K at 200 GPa. The graphenelike P layer and its coupling with La atoms dominate the superconducting origin of LaP₂H₂. On the other hand, LaP₂H₂ can achieve a superconducting transition at lower pressures compared with hydrides with a higher hydrogen content. The superconductivity in LaP₂H₂, LaPH, and LaPH₆ closely correlates with P motifs. This work will stimulate further experimental and theoretical studies to explore conventional superconductors with different building blocks.

The authors acknowledge funding from the Natural Science Foundation of China under Grants No. 21873017, No. 52022089, and No. 21573037, Natural Science Foundation of Hebei Province Grants No. A2019203507 and No. B2021203030, the Postdoctoral Science Foundation of China under Grant No. 2013M541283, and the Natural Science Foundation of Jilin Province (Grant No. 20190201231JC). This work was carried out at National Supercomputer Center in Tianjin, and the calculations were performed on TianHe-1 (A). A.B. acknowledges financial support from the Spanish Ministry of Science and Innovation (Grant No. PID2019-105488GB-I00).

-
- [1] A. P. Drozdov, M. I. Erements, I. A. Troyan, V. Ksenofontov, and S. I. Shylin, *Nature (London)* **525**, 73 (2015).
- [2] M. Somayazulu, M. Ahart, A. K. Mishra, Z. M. Geballe, M. Baldini, Y. Meng, V. V. Struzhkin, and R. J. Hemley, *Phys. Rev. Lett.* **122**, 027001 (2019).
- [3] H. Xie, Y. Yao, X. Feng, D. Duan, H. Song, Z. Zhang, S. Jiang, S. A. T. Redfern, V. Z. Kresin, C. J. Pickard *et al.*, *Phys. Rev. Lett.* **125**, 217001 (2020).
- [4] E. Snider, N. Dasenbrock-Gammon, R. McBride, M. Debessai, H. Vindana, K. Vencatasamy, K. V. Lawler, A. Salamat, and R. P. Dias, *Nature (London)* **586**, 373 (2020).
- [5] H. Liu, I. I. Naumov, R. Hoffmann, N. W. Ashcroft, and R. J. Hemley, *Proc. Natl. Acad. Sci. U.S.A.* **114**, 6990 (2017).
- [6] J. Bardeen, L. N. Cooper, and J. R. Schrieffer, *Phys. Rev.* **108**, 1175 (1957).
- [7] D. Duan, Y. Liu, F. Tian, D. Li, X. Huang, Z. Zhao, H. Yu, B. Liu, W. Tian, and T. Cui, *Sci. Rep.* **4**, 6968 (2014).
- [8] F. Peng, Y. Sun, C. J. Pickard, R. J. Needs, Q. Wu, and Y. Ma, *Phys. Rev. Lett.* **119**, 107001 (2017).
- [9] Y. Sun, J. Lv, Y. Xie, H. Liu, and Y. Ma, *Phys. Rev. Lett.* **123**, 097001 (2019).
- [10] N. P. Salke, M. M. D. Esfahani, Y. Zhang, I. A. Kruglov, J. Zhou, Y. Wang, E. Greenberg, V. B. Prakapenka, J. Liu, and A. R. Oganov, *Nat. Commun.* **10**, 1 (2019).
- [11] A. M. Shipley, M. J. Hutcheon, R. J. Needs, and C. J. Pickard, *Phys. Rev. B* **104**, 054501 (2021).
- [12] C. J. Pickard, I. Errea, and M. I. Erements, *Annu. Rev. Condens. Matter Phys.* **11**, 57 (2020).
- [13] A. R. Oganov, C. J. Pickard, Q. Zhu, and R. J. Needs, *Nat. Rev. Mater.* **4**, 331 (2019).
- [14] L. Zhang, Y. Wang, J. Lv, and Y. Ma, *Nat. Rev. Mater.* **2**, 17005 (2017).
- [15] J. Nagamatsu, N. Nakagawa, T. Muranaka, Y. Zenitani, and J. Akimitsu, *Nature (London)* **410**, 63 (2001).
- [16] J. Kortus, I. I. Mazin, K. D. Belashchenko, V. P. Antropov, and L. L. Boyer, *Phys. Rev. Lett.* **86**, 4656 (2001).
- [17] J. M. An and W. E. Pickett, *Phys. Rev. Lett.* **86**, 4366 (2001).
- [18] K. P. Bohnen, R. Heid, and B. Renker, *Phys. Rev. Lett.* **86**, 5771 (2001).
- [19] J. A. Flores-Livas, L. Boeri, A. Sanna, G. Profeta, R. Arita, and M. Erements, *Phys. Rep.* **856**, 1 (2020).
- [20] U. Pinsook, *J. Met Mater. Miner.* **30**, 31 (2020).
- [21] D. A. Papaconstantopoulos, B. M. Klein, M. J. Mehl, and W. E. Pickett, *Phys. Rev. B* **91**, 184511 (2015).
- [22] S. Yi, C. Wang, H. Jeon, and J.-H. Cho, *Phys. Rev. Mater.* **5**, 024801 (2021).
- [23] L. Liu, C. Wang, S. Yi, K. W. Kim, J. Kim, and J.-H. Cho, *Phys. Rev. B* **99**, 140501(R) (2019).
- [24] F. Bachhuber, J. von Appen, R. Dronskowski, P. Schmidt, T. Nilges, A. Pfitzner, and R. Wehrich, *Angew. Chem. Int. Ed.* **53**, 11629 (2014).
- [25] H. G. Von Schnering and W. Hönle, *Chem. Rev.* **88**, 243 (1988).
- [26] X. Liu, Z. Yu, Q. Liang, C. Zhou, H. Wang, J. Zhao, X. Wang, N. Yu, Z. Zou, and Y. Guo, *Chem. Mater.* **32**, 8781 (2020).
- [27] Y. Liu, C. Wang, X. Kong, and D. Duan, *Inorg. Chem.* **56**, 12529 (2017).
- [28] Y. Liu, C. Wang, P. Lv, H. Sun, and D. Duan, *Chem. Eur. J.* **24**, 11402 (2018).
- [29] A. Drozdov, M. Erements, and I. Troyan, [arXiv:1508.06224](https://arxiv.org/abs/1508.06224).

- [30] A. Shamp, T. Terpstra, T. Bi, Z. Falls, P. Avery, and E. Zurek, *J. Am. Chem. Soc.* **138**, 1884 (2016).
- [31] J. A. Flores-Livas, M. Amsler, C. Heil, A. Sanna, L. Boeri, G. Profeta, C. Wolverton, S. Goedecker, and E. K. U. Gross, *Phys. Rev. B* **93**, 020508(R) (2016).
- [32] H. Liu, Y. Li, G. Gao, J. S. Tse, and I. I. Naumov, *J. Phys. Chem. C* **120**, 3458 (2016).
- [33] Y. Yuan, Y. Li, G. Fang, G. Liu, C. Pei, X. Li, H. Zheng, K. Yang, and L. Wang, *Natl. Sci. Rev.* **6**, 524 (2019).
- [34] Z. Shao, D. Duan, Y. Ma, H. Yu, H. Song, H. Xie, D. Li, F. Tian, B. Liu, and T. Cui, *npj Comput. Mater.* **5**, 104 (2019).
- [35] X. Li, Y. Xie, Y. Sun, P. Huang, H. Liu, C. Chen, and Y. Ma, *J. Phys. Chem. Lett.* **11**, 935 (2020).
- [36] X. Guo, R.-L. Wang, H.-L. Chen, W.-C. Lu, K. M. Ho, and C. Z. Wang, *Phys. Lett. A* **384**, 126189 (2020).
- [37] S. Di Cataldo, W. von der Linden, and L. Boeri, [arXiv:2106.07266](https://arxiv.org/abs/2106.07266).
- [38] S. Di Cataldo, C. Heil, W. von der Linden, and L. Boeri, *Phys. Rev. B* **104**, L020511 (2021).
- [39] X. Liang, A. Bergara, X. Wei, X. Song, L. Wang, R. Sun, H. Liu, R. J. Hemley, L. Wang, G. Gao *et al.*, *Phys. Rev. B* **104**, 134501 (2021).
- [40] X. Chen, L. Zhu, and S. Yamanaka, *J. Solid State Chem.* **173**, 449 (2003).
- [41] Y. Wang, J. Lv, L. Zhu, and Y. Ma, *Phys. Rev. B* **82**, 094116 (2010).
- [42] W. Sun, X. Kuang, H. D. J. Keen, C. Lu, and A. Hermann, *Phys. Rev. B* **102**, 144524 (2020).
- [43] I. A. Kruglov, D. V. Semenok, H. Song, R. Szczeniński, I. A. Wrona, R. Akashi, M. M. D. Esfahani, D. Duan, T. Cui, and A. G. Kvashnin, *Phys. Rev. B* **101**, 024508 (2020).
- [44] F. Porsch and W. B. Holzapfel, *Phys. Rev. Lett.* **70**, 4087 (1993).
- [45] W. Chen, D. V. Semenok, I. A. Troyan, A. G. Ivanova, X. Huang, A. R. Oganov, and T. Cui, *Phys. Rev. B* **102**, 134510 (2020).
- [46] H. Katzke and P. Tolédano, *Phys. Rev. B* **77**, 024109 (2008).
- [47] C. J. Pickard and R. J. Needs, *Nat. Phys.* **3**, 473 (2007).
- [48] Y. Zhou, L.-T. Shi, A. K. Liang, Z.-Y. Zeng, X.-R. Chen, and H.-Y. Geng, *RSC Adv.* **11**, 3058 (2021).
- [49] See Supplemental Material at <http://link.aps.org/supplemental/10.1103/PhysRevB.105.024504> for computational details, phonon spectra and projected electronic band structures, electron density of states, Fermi surfaces and projected phonon densities of states and Eliashberg spectral functions, structural information of all stable La-P-H phases, and convex hulls of La-P system, which includes Refs. [50–60].
- [50] P. B. Allen and R. Dynes, *Phys. Rev. B* **12**, 905 (1975).
- [51] P. B. Allen and B. Mitrović, *Solid State Phys.* **37**, 1 (1983).
- [52] A. D. Becke and K. E. Edgecombe, *J. Chem. Phys.* **92**, 5397 (1990).
- [53] J. Carbotte, *Rev. Mod. Phys.* **62**, 1027 (1990).
- [54] G. Kresse and J. Furthmüller, *Phys. Rev. B* **54**, 11169 (1996).
- [55] J. P. Perdew, K. Burke, and M. Ernzerhof, *Phys. Rev. Lett.* **77**, 3865 (1996).
- [56] S. Baroni, S. de Gironcoli, A. Dal Corso, and P. Giannozzi, *Rev. Mod. Phys.* **73**, 515 (2001).
- [57] A. Togo, F. Oba, and I. Tanaka, *Phys. Rev. B* **78**, 134106 (2008).
- [58] P. Giannozzi, S. Baroni, N. Bonini, M. Calandra, R. Car, C. Cavazzoni, D. Ceresoli, G. L. Chiarotti, M. Cococcioni, I. Dabo *et al.*, *J. Phys.: Condens. Matter* **21**, 395502 (2009).
- [59] Y. Wang, J. Lv, L. Zhu, and Y. Ma, *Comput. Phys. Commun.* **183**, 2063 (2012).
- [60] H. Xiao, Y. Dan, B. Suo, and X. Chen, *J. Phys. Chem. C* **124**, 2247 (2020).
- [61] F. A. Cotton, *J. Chem. Phys.* **35**, 228 (1961).
- [62] R. W. Keyes, *Phys. Rev.* **92**, 580 (1953).
- [63] C.-H. Hu, A. R. Oganov, Q. Zhu, G.-R. Qian, G. Frapper, A. O. Lyakhov, and H.-Y. Zhou, *Phys. Rev. Lett.* **110**, 165504 (2013).
- [64] R. F. W. Bader, *Acc. Chem. Res.* **18**, 9 (1985).
- [65] K. Tanaka, J. S. Tse, and H. Liu, *Phys. Rev. B* **96**, 100502(R) (2017).
- [66] Y. Li, J. Hao, H. Liu, J. S. Tse, Y. Wang, and Y. Ma, *Sci. Rep.* **5**, 9948 (2015).
- [67] K. S. Grishakov, N. N. Degtyarenko, and E. A. Mazur, *J. Exp. Theor. Phys.* **128**, 105 (2019).
- [68] X. Liang, S. Zhao, C. Shao, A. Bergara, H. Liu, L. Wang, R. Sun, Y. Zhang, Y. Gao, Z. Zhao *et al.*, *Phys. Rev. B* **100**, 184502 (2019).
- [69] D. C. Lonie, J. Hooper, B. Altintas, and E. Zurek, *Phys. Rev. B* **87**, 054107 (2013).
- [70] Y. Sun, Y. Tian, B. Jiang, X. Li, H. Li, T. Iitaka, X. Zhong, and Y. Xie, *Phys. Rev. B* **101**, 174102 (2020).